Supplementary information

ASAXS study of the influence of sulfidation conditions and organic additives on sulfide slabs multiscale organization

S. Humbert [a]#, E. Devers [a], C. Lesage [a,b], C. Legens [a], L. Lemaitre [a], L. Sorbier [a], F. De Geuser [c], V. Briois [b]

[a]*IFP Energies nouvelles, Rond-point de l'échangeur de Solaize, BP 3, 69360 Solaize, France*

[b]*SOLEIL Synchrotron , BP48, L'Orme des Merisiers , Gif-Sur-Yvette , 91192 Saint-Aubin, France*

[c]*SIMaP, Grenoble INP, CNRS, Université Grenoble Alpes, 38000 Grenoble, France;*

#corresponding author

severine.humbert@ifpen.fr

Theoretical aspects of ASAXS

For the case of randomly oriented particles with identical shape and with size parameterized by R dispersed in a homogeneous matrix, the SAXS scattered intensity is given by:

$$I(q) = \frac{N_p}{V_s} \Delta\rho^2 \int_0^\infty P(R)V(R)^2|F(q,R)|^2\Psi(q,R)\mathrm{d}R \quad (1)$$

with N_p the number of particles, V_s the sample volume, $\Delta\rho^2$ the contrast factor such as:

$$\Delta\rho^2 = \left(\rho_p - \rho_m\right)^2 \quad (2)$$

ρ_p and ρ_m the scattering length densities of the particles and the matrix:

$$\rho = r_e \sum_j n_j f_j \quad (3)$$

n_j the number density of the atom j in the matrix or in the particles, f_j the atomic form factors and r_e the classical Thomson radius (r_e = 0.282 10^{-12} cm).

$P(R)$ is the size distribution function, $F(q,R)$ is the form factor and $\Psi(q,R)$ is the structure factor that equals to 1 when the particles are well spaced, i.e when distances between particles are larger than particle sizes.

For the case of metal particles supported on a porous alumina support, the SAXS analysis recorded at only one energy is not sufficient to distinguish the nanoparticles as the porous support also contributes significantly to the signal because of the scattering of the pores.

Hence, to isolate the signal specific for each phase, it is therefore mandatory to vary the energy of the incident beam and to perform the measurements near and far from the metal (molybdenum in our case) absorption edge.

It is recalled that the atomic form factor of a species j can be written:

$$f_j(E) = f_0 + f_j'(E) + if_j''(E) \qquad (4)$$

with $f_0 = Z$, the atomic number.

Resonant scattering method

The energy dependence of the radial scattering length density profile $\Delta\rho$ can be determined as [1–4]:

$$\Delta\rho(r,E) = \Delta\rho_0(r) + \nu(r)r_e\left[f_j'(E) + if_j''(E)\right] \qquad (5)$$

with $\Delta\rho_0(r)$ the non-resonant scattering length density profile (i.e. the usual contrast well below the absorption edge)and $\nu(r)$ the spatial distribution of anomalous scattering units (e.g. Mo species).

The total scattered intensity can then be expressed as

$$I(q,E) = F_0^2(q) + 2f_j'(E)F_0(q)\nu(q) + \left[f_j'^2(E) + f_j''^2(E)\right]\nu^2(q) \qquad (6)$$

with $F_0(q)$ and $\nu(q)$ the scattering amplitudes of normal and anomalous scattering units, respectively.

Finally, $I(q)$ contains three components: the energy-independent normal SAXS, a cross-term involving the amplitude of normal SAXS and the resonant scattering of the molybdenum atoms, and the pure resonant scattering term due to the molybdenum atoms.

Subtraction method

A second method can also be carried out in order to extract the signal specific for the molybdenum phase.

Considering a system of particles p supported on a porous support s and with air filling the pores, the scattered intensity can be written thanks to the partial structure factors S_{pp}, S_{ss} and S_{sp} described by Binninger et al. [5] as follow:

$$\langle I(q,E)\rangle = |f_s|^2 n_s^2 r_e^2 S_{ss}(q) + 2\Re\left(f_p(E) f_s^*\right) n_p n_s\, r_e^2 S_{sp}(q) + \left|f_p(E)\right|^2 n_p^2 r_e^2 S_{pp}(q) \qquad (7)$$

where $\Re$ is the real part and * the complex conjugate. Notice the similarity of the terms of equation (7) with the ones of equation (6).

In the aim to simplify the writing of the following equations and to be coherent with literature notation on this subject [6–8], the electronic density of the particles and the porous support $\sum_j n_j f_j$ are noted , $n_p f_p$ and $n_s f_s$.

Neglecting the imaginary parts of both f_s and f_p, the difference between the intensities measured at two different energies E_1 and E_2 leads to:

$$\begin{aligned}\langle I(q,E_i)\rangle - \langle I(q,E_j)\rangle &= n_p^2 r_e^2 \left(\left|f_p(E_i)\right|^2 - \left|f_p(E_j)\right|^2\right) S_{pp}(q) + 2 f_s \left(f_p(E_i) - f_p(E_j)\right) n_p n_s r_e^2 S_{sp}(q) \\ &= n_p^2 r_e^2 \left(\left|f_p(E_i)\right|^2 - \left|f_p(E_j)\right|^2\right).\left(S_{pp}(q) + \alpha S_{sp}(q)\right)\end{aligned} \qquad (8)$$

where $\overline{f_p} = \frac{f_p(E_i)+f_p(E_j)}{2}$ is the mean value of $f_p(E)$ and $\alpha = \frac{n_s f_s}{n_p \overline{f_p}}$

For independent spherical metallic particles deposited on spherical particle of support we have:

$$S_{pp}(q) = \frac{N_p}{V_s} \int_0^{+\infty} P_p(R_p) V_p^2(R_p)\, F_p^2(q,R_p) dR_p \qquad (9)$$

$$S_{sp} = \frac{N_p}{V_s} \iint_0^{\infty} P_p(R_p) P_s(R_s) V_p(R_p) V_s(R_s) F_p(q,R_p) F_s(q,R_s) \frac{\sin\left(q(R_p+R_s)\right)}{q(R_p+R_s)}\, \mathrm{d}R_p \mathrm{d}R_s \qquad (10)$$

In our case, α ~ 0.83 so the interference term S_{sp} is maybe not negligible. Both terms should therefore be taken into account for the data modeling.

Interest of ASAXS

An example of SAXS curves of a sulfide catalyst obtained at E_1 = 19700 eV and E_3 = 19990 eV is given in Figure 1, in the form of $i(q) = q^2 I(q)$ in order to exacerbate differences. It can be noticed that the gap between both SAXS curves is very tiny, which underlines the importance to carry out careful analysis and calibration. The respective ASAXS curve obtained from the subtraction of the intensity measured at E_1 = 19700 eV and the intensity measured at E_3 = 19990 eV is also plotted on Figure 1. One can notice that the global shape of SAXS and ASAXS curves is different, due to the fact that the SAXS response depends on

both alumina support and molybdenum particles. Moreover, the main interest of ASAXS is demonstrated by the Figure 2 on which the SAXS and ASAXS curves are plotted for the TEG-gas and Dried-gas samples. The SAXS signals of the two catalysts are very close, while the ASAXS signals make it possible to exacerbate their small differences and so to differentiate them much better.

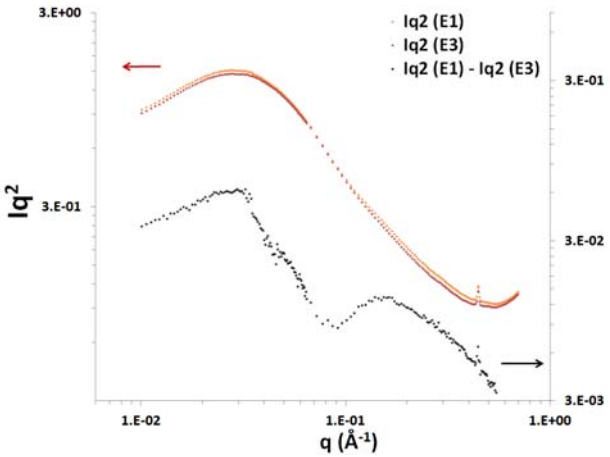

Figure 1. $q^2I(q)$ curves obtained at E_1 (19700 eV) and E_3 (19990 eV) and the ASAXS curve obtained from the subtraction $q^2I(q,E_1) - q^2I(q,E_3)$ for the TEG-gas catalyst.

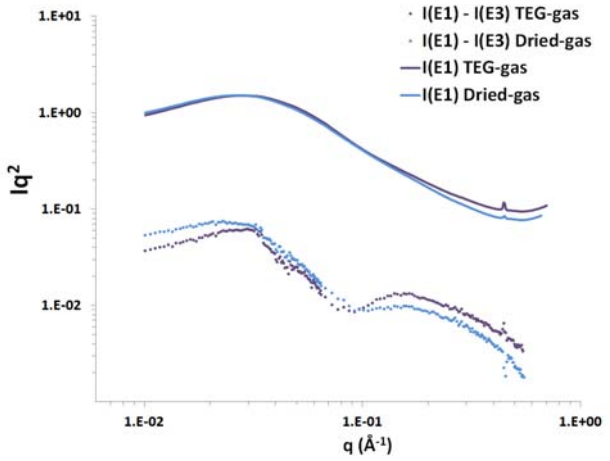

Figure 2. $q^2I(q)$ SAXS curves obtained at E_1 (19700 eV) and the ASAXS curves obtained from the subtraction $q^2I(q,E_1) - q^2I(q,E_3)$ for the TEG-gas and Dried-gas catalysts.

ASAXS data modeling

To evaluate the size distribution of the sulfided slabs, a nonlinear least-squares adjustment of the ASAXS signal is performed on equation (8). The assumptions made for the choice of the regression model are listed below.

Morphology and size distribution of molybdenum phase

Given the shape of the curves (two inflections of the scattered signal), the experimental data could not be fitted with only one function of size distribution. It appears that two kinds of molybdenum objects exist in the catalyst, at two different scales. Based on the electron microscopy observations, these two populations can be attributed to isolated slab stacks at the small scale, and to larger, polycrystalline and moderately dense slab aggregates at larger scale.

For the molybdenum phase, we thus consider that the scattering objects can be porous. We call the porosity ε. In the case of crystalline slabs, ε = 0 and in the case of slab aggregates, ε > 0.

The number of molybdenum atoms in the scattering object is defined by [9]:

$$N_{Mox} = \frac{N_A \times \rho_{\mathrm{Mo_x}}}{M_{\mathrm{Mo_x}}} \times V \times (1-\varepsilon) \qquad (11)$$

with Mo_x = MoS_2 in the case of sulfided molybdenum and Mo_x = MoO_y in the case of oxide molybdenum, V the volume of the scattering object, N_A the Avogadro's number (6.022×10^{23} mol^{-1}), $M_{\mathrm{Mo_x}}$ the molar mass in g/mol and $\rho_{\mathrm{Mo_x}}$ the density in g/cm^3 of the molybdenum phase.

Hence, the scattering factor of a molybdenum object is defined by:

$$n_p f_p = \left(\frac{N_A \times \rho_{\mathrm{Mo_x}}}{M_{\mathrm{Mo_x}}} \times f_{Mox}\right) \times (1-\varepsilon) \qquad (12)$$

The term $\frac{N_p}{V_s}$ of the equation (9) can be expressed as:

$$\frac{N_p}{V_s} = \frac{w_{\mathrm{Mo_x}} \times \rho_s}{\rho_{\mathrm{Mo_x}}} \times \frac{1}{1-\varepsilon} \times \frac{1}{\langle V \rangle} \qquad (13)$$

With $\langle V \rangle$ the mean volume of the slab stack or slab aggregate (cm^{-3}), $w_{\mathrm{Mo_x}}$ the weight concentration of the molybdenum phase (wt.%), ρ_s the sample structural density in g/cm^3.

Slab stacks are considered to be isolated as the total volume fraction is very low: therefore, the structure factor at small q is not taken into account while the form factor is.

Stacked slabs can be modeled as discs of height $2H$ and radius R_p.

The form factor for disc-like particles of radius R_p and height $2H$ is [10,11]:

$$F_{disc}^2(q, R_p, H) = 4\int_0^{\pi/2} \left(\frac{\sin^2(qH\cos\beta)}{(qH)^2\cos^2\beta}\right) \frac{J_1^2(qR_p\sin\beta)}{(qR_p)^2\sin^2\beta} \sin\beta \, \mathrm{d}\beta \qquad (14)$$

and

$$V_p(R_p, H) = \pi {R_p}^2 2H \qquad (15)$$

Slab aggregates can be modeled as ellipsoids of revolution (a spheroid) of axes (R_a, R_a and νR_a).

The form factor for spheroidal object is:

$$F^2_{ellipsoid}(q, R_a, \nu) = \int_0^1 \Phi^2[qR_a(1 + x^2(\nu^2 - 1))^{0.5}]\,\mathrm{d}x \quad (16)$$

and

$$\Phi(t) = 3\left(\frac{\sin t - t\cos t}{t^3}\right) \quad (17)$$

and

$$V_a(R_a, \nu) = \frac{4}{3}\pi\nu {R_a}^3 \quad (18)$$

The size distributions of slabs and aggregates are represented by log-normal distributions:

$$P_k(R_k) = \frac{1}{\sqrt{2\pi}R_k\sigma_k}\exp\left(-\frac{(\ln R_k - \mu_k)^2}{2\sigma_k^2}\right) \quad (19)$$

Where k equals to p for slab stacks and equals to a for the aggregates, and μ and σ are respectively the scale and the shape parameters of the lognormal law.

The size distribution of slab stacks modeled by discs concerns only the radius dimension R_p (the thickness $2H$ is monodisperse), and the size distribution of slab aggregates modeled by a spheroid concerns only the axes R_a (ν takes a single value, so the aspect ratio is fixed).

In order to calculate the number and volume average sizes from the adjusted log-normal distribution, the distribution moments M_n must be known [12]:

$$M_{n_k} = \exp\left(\mu_k \times n + \frac{n^2{\sigma_k}^2}{2}\right) \quad (20)$$

The volume size distributions P_{pv} and P_{av} respectively for disc-like particles and ellipsoidal aggregates are defined by:

$$P_{pv}(R_p) = \frac{{R_p}^2 P_p(R_p)}{M_{2p}} \quad (21)$$

$$P_{av}(R_a) = \frac{{R_a}^3 P_a(R_a)}{M_{3a}} \quad (22)$$

The number and the volume averaged size of the slabs can be calculated:

$$Rp_{num} = \frac{M_{1p}}{M_{0p}} = \exp\left(\mu_p + \frac{\sigma_p^2}{2}\right) \text{ and } Rp_{vol} = \frac{M_{3p}}{M_{2p}} = \exp\left(\mu_p + \frac{5\sigma_p^2}{2}\right) \quad (23)$$

And the number and the volume averaged size of the aggregates can be calculated:

$$Ra_{num} = \frac{M_{1a}}{M_{0a}} = \exp\left(\mu_a + \frac{\sigma_a^2}{2}\right) \text{ and } Ra_{vol} = \frac{M_{4a}}{M_{3a}} = \exp\left(\mu_a + \frac{7\sigma_a^2}{2}\right) \quad (24)$$

Finally, the term S_{pp} reads:

$$S_{pp}(q) = \left[\frac{N_{pp}}{V_s}\int_0^{+\infty} P_p(R_p)\ V_p^2(R_p,H)F_{disc}^2(q,R_p,H)\mathrm{d}R_p + \frac{N_{pa}}{V_s}\int_0^{+\infty} P_a(R_a)V_a^2(R_a,\nu)F_{ellipsoid}^2(q,R_a,\nu)\,\mathrm{d}R_a\right] \quad (25)$$

with

$$\frac{N_{pp}}{V_s} = \frac{w_{Mox}\times\rho_s}{\rho_{Mox}} \times w_p \times \frac{1}{1-\varepsilon_p} \times \frac{1}{\langle V_p\rangle} \text{ and } \frac{N_{pa}}{V_s} = \frac{w_{Mox}\times\rho_s}{\rho_{Mox}} \times w_a \times \frac{1}{1-\varepsilon_a} \times \frac{1}{\langle V_a\rangle} \quad (26)$$

where w_p and w_a are the fraction of molybdenum in slabs and aggregates, respectively and $\langle V_p \rangle$ and $\langle V_a \rangle$ are the mean volumes of the slabs and the aggregates, respectively such as :

$$\langle V_p\rangle = \pi \times 2H \times \int {R_p}^2 P_p(R_p)\mathrm{d}R_p = \pi \times M_{2_p} \times 2H = \pi \times 2H \times \exp\left(2\mu_p + \frac{4\sigma_p^2}{2}\right) \quad (27)$$

$$\langle V_a\rangle = \frac{4}{3} \times \pi \times \nu \times \int {R_a}^3 P_a(R_a)\mathrm{d}R_a = \frac{4}{3} \times \pi \times \nu \times M_{3_a} = \frac{4}{3} \times \pi \times \exp\left(3\mu_a + \frac{9\sigma_a^2}{2}\right) \quad (28)$$

Interference between molybdenum phase and support

To take into account the interference between molybdenum phase and the alumina support and to calculate the S_{sp} term of the equation (8), the size distribution $P_s(R_s)$, the particle volume $V(R_s)$ and the form factor $F(q,R_s)$ have to be defined. Hence, pure alumina support has been analyzed by SAXS to determine these different terms. The support structure can thus be described by:

$$F_s(q,R_s) = 3\left(\frac{\sin qR_s - qR_s\cos qR_s}{(qR_s)^3}\right) \quad (29)$$

$$V_s(R_s) = \frac{4}{3}\pi {R_s}^3 \quad (30)$$

And with a bimodal lognormal distribution such as:

$$P_s(R_s) = \frac{1}{\mathrm{C}_1+\mathrm{C}_2}\left(\mathrm{C}_1 \times P_{s1}(R_s) + \mathrm{C}_2 \times P_{s2}(R_s)\right) \quad (31)$$

With $\mathrm{C}_1 = 1$ and $\mathrm{C}_2 = 0.21$, $\mu_{s1} = 2.88$, $\sigma_{s1} = 0.33$, $\mu_{s2} = 2.74$ and $\sigma_{s2} = 0.69$

Final model

Supposing that the first particle population corresponds to dense, crystalline and isolated stacked slabs and that the second one is attributed to aggregates partially dense, the equation (8) becomes:

$$\langle I(q,E_i)\rangle - \langle I\big(q,E_j\big)\rangle = w_{\mathrm{Mo_x}} \times w_p \times \frac{\rho_s}{\rho_{\mathrm{Mo_x}}} \times \Delta^2_{\mathrm{Mo_x}}\big(E_i,E_j\big) \times \big(S'_{pp} + \alpha S'_{sp}\big) \qquad (32)$$

with

$$\Delta^2_{\mathrm{Mo_x}}\big(E_i,E_j\big) = {r_e}^2 \times \left[\Big(n_{\mathrm{Mo_x}} f_{\mathrm{Mo_x}}(E_i)\Big)^2 - \Big(n_{\mathrm{Mo_x}} f_{\mathrm{Mo_x}}\big(E_j\big)\Big)^2\right] \qquad (33)$$

$$S'_{pp}(q) = \left[\frac{1}{< V_p >}\int_0^{+\infty} P_p\big(R_p\big)\ V_p^2\big(R_p,H\big)F_{disc}^2\big(q,R_p,H\big)\mathrm{d}R_p + \frac{w_a(1-\varepsilon_a)}{w_p} \times \frac{1}{< V_a >}\int_0^{+\infty} P_a(R_a)V_a^2(R_a,\nu)F_{ellipsoid}^2(q,R_a,\nu)\,\mathrm{d}R_a\right] \qquad (34)$$

$$S'_{sp}(q) = \left[\frac{1}{<V_p>}\iint_0^{\infty} P_s(R_s)V_s(R_s)F_s(q,R_s)P_p\big(R_p\big)V_p\big(R_p,H\big)F_{disc}\big(q,R_p,H\big)\frac{\sin\big(q(R_p+R_s)\big)}{q(R_p+R_s)}\mathrm{d}R_p\mathrm{d}R_s + \frac{w_a(1-\varepsilon_a)}{w_p} \times \frac{1}{<V_a>}\iint_0^{\infty} P_s(R_s)V_s(R_s)F_s(q,R_s)P_a(R_a)V_a(R_a,\nu)F_{ellipsoid}(q,R_a,\nu)\frac{\sin\big(q(R_a+R_s)\big)}{q(R_a+R_s)}\mathrm{d}R_a\mathrm{d}R_s\right] \qquad (35)$$

Obtained parameters

This model allows estimating the length distribution of the slabs (μ_p, σ_p), the size distribution of the aggregates (μ_a, σ_a) and the parameter $\frac{w_a(1-\varepsilon_a)}{w_p}$ which depends on the ratio between the molybdenum content included in the first and in the second population, but also on the porosity of the aggregates.

In particular, two parameters can be used to describe the slabs:

- The mean length (in number) $\boldsymbol{L_{slabs}}$ such as :

$$L_{slabs} = 2 \times R_{pnum} \qquad (36)$$

- The stacking state $\boldsymbol{z_{slabs}}$ such as :

$$z_{slabs} = \frac{2H}{3.1} \qquad (37)$$

3.1 Å being the thickness of one slab according to crystallography [13]. Hence, $z = 1$ when it is a mono-slab and $z = 3$ for a two-stack slabs. The number averaged length is considered here so that it could be easily compared to the mean length measured in TEM.

Three parameters are useful to describe the slab aggregates:

- The aggregate width $\boldsymbol{W_{ag}}$ such as :

$$W_{ag} = 2 \times R_{avol} \quad (38)$$

- The aggregate length $\boldsymbol{L_{ag}}$ such as :

$$L_{ag} = 2 \times \upsilon \times R_{avol} \quad (39)$$

This aggregate length is however subject to significant uncertainties as the ASAXS curves are not very sensitive to length differences for lengths up to 50 nm.

- The parameter $\boldsymbol{C_{ag}}$ such as :

$$w\mathcal{E} = \frac{w_a(1-\varepsilon_a)}{w_p} \; and \; C_{ag} = \frac{w\mathcal{E}}{1+w\mathcal{E}} \quad (40)$$

This parameter traduces roughly the aggregate content (in percent): the higher C_{ag} is, the more aggregated the slabs are, and so the lower the dispersion is.

Comparison of both methods

Both method have been carried out for the TEG-gas sample. The three subtraction $I(E_1)$-$I(E_2)$, $I(E_1)$-$I(E_3)$ and $I(E_2)$-$I(E_3)$ are plotted on Figure 3. From a global point of view, the three curves present similar shape. Just small differences are observed, either due to interference term or experimental uncertainties.

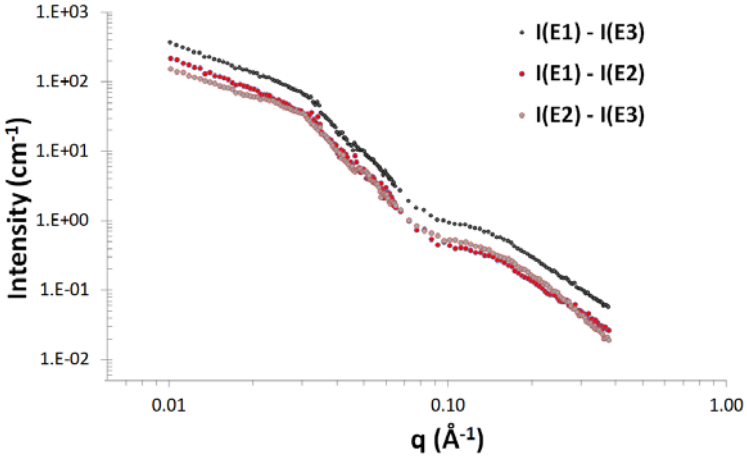

Figure 3. ASAXS curves obtained from the subtractions $I(E_1)$-$I(E_2)$, $I(E_1)$-$I(E_3)$ and $I(E_2)$-$I(E_3)$.

Calculation of pure resonant scattering

The pure resonant scattering term was evaluated from both method, using the *SAXSutilities* software of Sztucky et al. [1] for the first method, and by calculating the term S_{pp} for the second method using Matlab®. Resulting curves are plotted on Figure 4.

The same general shape is obtained from both methods. However we can notice that the signal obtained by the first method is quite noisy in the q-range of 6.10^{-2} Å^{-1} – 10^{-1} Å^{-1}, which can be problematic for the signal modeling. This is possibly due to the fact that only three energies are maybe not sufficient to obtain a sufficient accuracy with this method, or also to the uncertainties on the scattering factors f' and f". Indeed, the molybdenum is mainly in the form of MoS_2, which impact the position of the K-edge of absorption and the values of scattering factors.

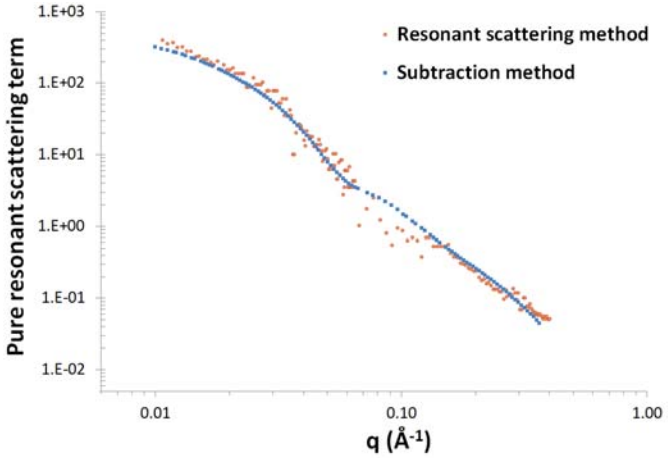

Figure 4. Pure resonant scattering term obtained with both method: $\nu(q)$ of equation (6) and the term S_{pp} of equation (8).

Hence, the subtraction method was chosen to extract the resonant term S_{pp} and the interference term S_{sp}.

Calculation of interference term

In order to minimize the uncertainties, partly due to the subtraction of two very close intensities, it made more sense to use $I(E_1)$-$I(E_3)$ to extract the morphological data.

S_{pp}, S_{sp} and the combination of both term for the TEG-gas sample are plotted on Figure 5. The contribution of the interference term is negligible, except in the q-range of 6.10^{-2} Å^{-1} – 10^{-1} Å^{-1}. It is thus important to take it into account, especially for the determination of the slab stacks properties. To the contrary, slab aggregates scale is slightly affected by the interference term.

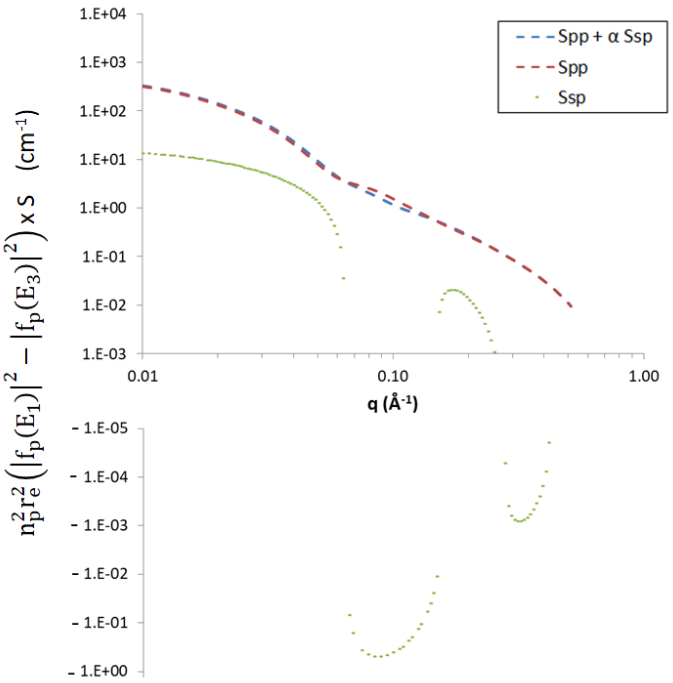

Figure 5. Pure resonant scattering S_{pp}, interference term S_{sp} and the combination of both.

Example of fit

An example of fit is presented in Figure 6 for the TEG-gas sample. The first part of the curve (from 10^{-1} Å^{-1} to 1 Å^{-1}) is essentially due to the contribution of the first population of small-size slabs (pure resonant scattering plus interference) whereas the second part of the curve (from 10^{-2} Å^{-1} to 10^{-1} Å^{-1}) is due to the contribution of the second population of larger objects called aggregates.

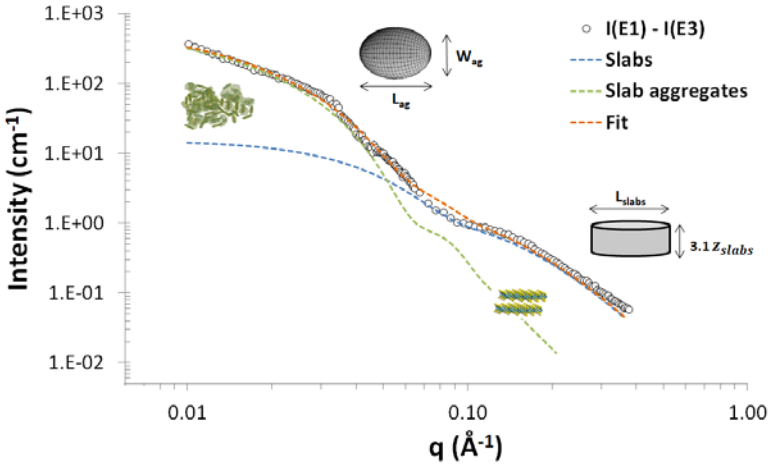

Figure 6. ASAXS curve obtained on the TEG-gas catalyst and fit of the experimental ASAXS data.

Comparison of results obtained from the three curves $I(E_1)$-$I(E_2)$, $I(E_1)$-$I(E_3)$ and $I(E_2)$-$I(E_3)$

Data modeling of the TEG-gas sample has been carried out on the three curves $I(E_1)$-$I(E_2)$, $I(E_1)$-$I(E_3)$ and $I(E_2)$-$I(E_3)$, in order to evaluate the uncertainties of the method. Results are reported in Table 1. The standard deviation is relatively small for the fourth parameters (z_{slabs}, L_{slabs}, C_{ag} and W_{ag}). Furthermore, the values obtained from the $I(E_1)$-$I(E_3)$ subtraction are the closest to the mean values. Consequently, $I(E_1)$-$I(E_3)$ curves have been chosen for the data modeling of all samples.

It should also be noticed that the L_{ag} values vary a lot depending on the considered subtraction. It is very sensitive to small variation at small q. Moreover, the ASAXS curves are not very sensitive to length differences for lengths up to 50 nm. Consequently, this parameter should not be considered for the comparison of the different samples because of its lack of accuracy.

Table 1. Results obtained on TEG-gas sample by fitting the three different ASAXS curves with the multi-scale model.

Subtraction	z_{slabs}	L_{slabs} (nm)	C_{ag} (%)	W_{ag} (nm)	L_{ag} (nm)
E_1-E_3	**2.8**	**4.9**	**32%**	**13.2**	**47**
E_2-E_3	**3.0**	**4.8**	**27%**	**15.1**	**20**
E_1-E_2	**2.5**	**5.0**	**36%**	**13.2**	**86**
Mean	**2.8**	**4.9**	**32%**	**13.8**	**51**
SD	**0.24**	**0.11**	**4.6%**	**1.10**	**33**

References

[1] M. Sztucki, E. Di Cola, T. Narayanan, Instrumental developments for anomalous small-angle X-ray scattering from soft matter systems, Journal of Applied Crystallography 43 (2010) 1479–1487. https://doi.org/10.1107/S002188981003298X.

[2] M. Sztucki, E. Di Cola, T. Narayanan, New opportunities for Anomalous Small-Angle X-Ray Scattering to characterize Charged Soft Matter Systems, in: A. Takahara, K. Sakurai (Eds.), Future trends in soft materials research with advanced light sources, 2011.

[3] H.B. Stuhrmann, Resonance scattering in macromolecular structure research, in: H.H. Kausch, H.G. Zachmann (Eds.), Characterization of Polymers in the Solid State II: Synchrotron Radiation, X-ray Scattering and Electron Microscopy, Springer Berlin Heidelberg, Berlin, Heidelberg, 1985, pp. 123–163.

[4] S. Haas, A. Hoell, G. Zehl, I. Dorbandt, P. Bogdanoff, S. Fiechter, Structural Investigation of Carbon Supported Ru-Se Based Catalysts using Anomalous Small Angle X-Ray Scattering, ECS Transac 6 (2008). https://doi.org/10.1149/1.2943231.

[5] T. Binninger, M. Garganourakis, J. Han, A. Patru, E. Fabbri, O. Sereda, R. Kötz, A. Menzel, T.J. Schmidt, Particle-Support Interferences in Small-Angle X-Ray Scattering from Supported-Catalyst Materials, Phys. Rev. Applied 3 (2015). https://doi.org/10.1103/PhysRevApplied.3.024012.

[6] H.G. Haubold, X.H. Wang, G. Goerigk, W. Schilling, In situ anomalous small-angle X-ray scattering investigation of carbon-supported electrocatalysts, J. Appl. Crystallogr. 30 (1997) 653–658. https://doi.org/10.1107/s0021889897002422.

[7] H.G. Haubold, X.H. Wang, ASAXS studies of carbon-supported electroctalysts, Nuclear Instruments & Methods in Physics Research Section B-Beam Interactions with Materials and Atoms 97 (1995) 50–54.

[8] F. Wen, N. Waldofner, W. Schmidt, K. Angermund, H. Bonnemann, S. Modrow, S. Zinoveva, H. Modrow, J. Hormes, L. Beuermann, S. Rudenkiy, W. Maus-Friedrichs, V. Kempter, T. Vad, H.G. Haubold, Formation and characterization of Pt nanoparticle networks, European Journal of Inorganic Chemistry (2005) 3625–3640. https://doi.org/10.1002/ejic.200500446.

[9] S. Humbert, G. Desjouis, T. Bizien, L. Lemaitre, A.L. Taleb, C. Dalverny, L. Sorbier, A.S. Gay, Effect of reduction on Co catalyst active phase highlighted by an original approach coupling ASAXS and electron tomography, Journal of Catalysis 366 (2018) 202–212. https://doi.org/10.1016/j.jcat.2018.07.024.

[10] Guinier A, Fournet G, Small-Angle Scattering of X-Rays, Wiley, New York, 1955.

[11] D.I. Svergun, M.H.J. Koch, Small-angle scattering studies of biological macromolecules in solution, Reports on Progress in Physics 66 (2003) 1735–1782.

[12] C.S. Forbes, Statistical distributions, 4th ed., Wiley, Hoboken, N.J., 2011.

[13] E.S. Kadantsev, P. Hawrylak, Electronic structure of a single MoS2 monolayer, Solid State Communications 152 (2012) 909–913. https://doi.org/10.1016/j.ssc.2012.02.005.